Energy 183 (2019) 983–995

Contents lists available at ScienceDirect

Energy

journal homepage: www.elsevier.com/locate/energy

Wind farm layout optimization for wake effect uniformity

Kyoungboo Yang [a, *], Gyeongil Kwak [b], Kyungho Cho [c], Jongchul Huh [d, **]

[a] Faculty of Wind Energy Engineering, Jeju National University, 102 Jejudaehakno, Jeju, Republic of Korea
[b] Renewable Energy (Wind Energy), Energy Division, Lahmeyer International, Germany
[c] Department of Mechatronics Engineering, Jeju National University, 102 Jejudaehakno, Jeju, Republic of Korea
[d] Department of Mechanical Engineering, Jeju National University, 102 Jejudaehakno, Jeju, Republic of Korea

ARTICLE INFO

Article history:
Received 6 April 2019
Received in revised form
18 June 2019
Accepted 2 July 2019
Available online 4 July 2019

Keywords:
Wind energy
Wind farm layout optimization
Simulated annealing algorithm
Energy maximization
Wake effect uniformity

ABSTRACT

The basic objective of wind farm layout optimization is to maximize the energy produced by wind farms. However, when wind turbines are arranged in a limited space like an onshore wind farm, specific wind turbines may have greater wake exposure than other wind turbines. This phenomenon can be conspicuous in a mixed layout that consists of turbines with different capacities and hub heights. In this study, we developed and tested a new objective function to increase wind farm energy output while making the wake loss of each wind turbine uniform. The purpose of this function is to adjust the wake effects of all of the wind turbines on a wind farm to similar levels, thereby promoting the operational stability of all of the wind turbines. Layout optimization was performed using a simulated annealing algorithm, which is a heuristic method, with actual wind conditions for an existing wind farm in operation. Then, the results obtained using the proposed method were compared with those yielded by layout optimization for energy maximization. The layout generated using the proposed objective function had lower energy output than that obtained by energy maximization. However, this difference was small and the proposed method prevented wake effect concentration on specific turbines by making the wake effect levels uniform.

1. Introduction

The main objective in wind farm design is energy output maximization. To achieve this objective, the losses must be minimized while maximizing the energy generated by the wind farm. The greatest losses are called wake losses, which are caused by wakes and result from the mutual interference between wind turbines. As wind consumes energy while passing through the rotor of a wind turbine, its speed is lower behind the turbine, which decreases the outputs of other downstream wind turbines [1]. Furthermore, an arrangement of wind turbines in a row along the wind direction causes additional wind speed and power output reduction. These reductions of wind speed and energy output are related to the problem of how to arrange wind turbines on a wind farm. To solve this problem, an effective wind farm layout is required to minimize the wake losses [2].

To minimize the wake losses, the turbines must be arranged considering the directions of all of the winds around the wind farm. However, numerous layout options are necessary for this purpose, making determination of the optimal wind turbine layout an extremely difficult task. The problem becomes more complicated if constraints present when turbines are actually arranged are considered, such as the presence of power cables, development-prohibited areas, and geographical characteristics.

As shown in Table 1, many studies have been conducted from the 1990s until recently to solve the problem of wind farm layout optimization (WFLO). The first report was published in 1994 by Mosetti et al. [3], who addressed the WFLO problem using a GA based on a discrete model. Mosetti et al. assumed and applied three simple wind conditions, which are different from those in actual situations, but nonetheless demonstrated the applicability of an optimization algorithm to solve the WFLO problem. After that, WFLO research ceased, but it started again in the mid-2000s. In 2004, Ozturk et al. [4] published a report on wind turbine layout optimization using a GHA. Grady et al. [5] investigated the same example as Mosetti et al. by employing a GA that introduced a subpopulation and compared the results. Marmidis et al. [6] introduced MCS, and Rivas et al. [7] conducted a study on WFLO

* Corresponding author.
** Corresponding author.
E-mail addresses: kbyang@jejunu.ac.kr (K. Yang), jchuh@jejunu.ac.kr (J. Huh).

https://doi.org/10.1016/j.energy.2019.07.019
0360-5442/

Nomenclature

AEP	annual energy production
LOEM	layout optimization for energy maximization
LOWU	layout optimization for wake effect uniformity
SAA	simulated annealing algorithm
STD	standard deviation
WFLO	wind farm layout optimization
WT	wind turbines
$A_{overlap}$	overlap area between wake and rotor [m^2]
$A_{partial}$	overlap area created by partial wake [m^2]
A_r	wind turbine rotor swept area [m^2]
C_t	thrust coefficient [−]
D_r	turbine rotor diameter [m]
D_w	diameter of the downstream wake [m]
E_{net}	net AEP [GWh]
E_{gross}	gross AEP [GWh]
F	probability of wind speed [−]
$f_{enery,max}$	value of objective function for energy maximization [−]
$f_{wake,uniform}$	value of objective function for wake effect uniformity [−]
$_{hhub}$	hub height of the wind turbine [m]
k_w	wake decay constant [−]
L	layout result of wind turbines
P	power of wind turbine [kW]
P_{metro}	metropolis probability [−]
u	wind speed [m/s]
u_{def}	wind speed deficit [m/s]
u_{mdef}	wind speed deficit by multiple WT [m/s]
T	virtual temperature parameter [−]
T_i	virtual temperature parameter, iteration step i [−]
$_{z0}$	surface roughness height [m]
α	temperature control parameter [−]

using an SAA. Before 2010, research was focused on the development of a layout optimization algorithm using various optimization methodologies. Furthermore, the investigations remained at the level of reviewing the applicability of the algorithms using rectangular wind farm areas and simple wind conditions.

Since 2010, more practical studies have been conducted using more diverse algorithms. The methodologies used in these studies can be categorized into two main types, as shown in Table 1: heuristic methodologies based on probabilistic theory [3–41] and mathematical programming methodologies involving formulating the variables and boundary conditions of the problem [42–51]. It can be seen from Table 1 that many studies related to WFLO have involved attempts to solve the problem using heuristic methodologies. That is because the WFLO problem is a combinatorial optimization problem, which is treated as an NP-hard problem due to its computational complexity and numerous constraints, which make it difficult to express a perfect mathematical function to find the optimal solution [10,51]. On the other hand, to overcome the problems of the probabilistic heuristic approach, such as the lack of a guarantee of global optimality and high computational cost, other researchers have approached the WFLO problem using mathematical programming methods such as MIP [42–46] and GBO [47–51]. However, some scholars believe that using mathematical programming for wind farm designing is not a good idea because of the non-linear, multi-modal, and discontinuous nature of the WFLO problem [52,53]. In this study, the heuristics method was adopted to account for the aforementioned nature of the WFLO problem.

There are also studies involving the use of complex algorithms that include both of the above-mentioned methods. Perez et al. [54] employed a random heuristic method for the initial layout of an offshore wind farm and applied nonlinear mathematical programming for local optimization. Mittal et al. [55] determined the number and positions of wind turbines by developing a hybrid methodology that combines a GA and GBO.

Examination of the applied algorithms indicates that population-based, nature-inspired algorithms, such as GAs [3,5,8–22], ESs [26–28], PSOs [22,29–34], and ACO [35], have been used often, and GAs have been used the most frequently. GAs are representative stochastic optimization algorithms that are used widely in various fields. GAs are advantageous due to their use of population-based cooperation systems, but the optimal solution depends on the chosen numbers of populations and generations, as well as the selection and crossover method, and it is difficult to make decisions about these factors. Other studies involving heuristic methods include one in which an SAA was employed to simulate the annealing process to improve the ductility of metal materials [7], and ones in which algorithms based on natural searches such as HS [36], PS [37], and RSs [38–40] were applied. Furthermore, GHAs [4,10,41], which are deterministic-based heuristic methods, have been applied to the WFLO problem in some studies.

For wind farm modeling, computational domains can be classified as grid-based discrete representations and coordinate-based continuous representations. Discrete representations are used to divide wind farms into rectangular grids and place wind turbines at the centers of the divided cells. This representation method is disadvantageous in that the degree of freedom of wind turbine placement varies with the grid resolution, and the computation time increases exponentially when a high-resolution grid is employed to increase the positional freedom [49]. On the other hand, in the continuous representation, wind turbines can be placed anywhere on the wind farm based on 2D coordinates [44]. As shown in Table 1, the computational domain generally depends on the algorithm. In the case of a GA, a discrete representation is advantageous due to the binary coding method, and in the case of an ES, in which real number operators are used, a continuous representation is employed. Similarly, the discrete and continuous representations are applied in MIP and GBO, respectively, depending on the characteristics of the algorithm.

Recently, various objective functions reflecting the actual conditions of real wind farms have been researched. Gonzalez et al. [13] conducted layout optimization considering the effects of grouping neighboring offshore wind farms that have been developed actively in recent years. Hou et al. [34] performed layout optimization to minimize the costs of configuring the substations and cables of offshore wind farms using an objective function based on the levelized production cost. Guirguis et al. [49] performed multi-objective layout optimization to achieve various design objectives including electrical infrastructure, land footprint, and land use. Tingey et al. [50] investigated the trade-offs between power production and noise impact using an acoustic model for noise, which is often an issue in wind farm development. Future research on WFLO is expected to reflect real problems actively, and this aspect was also considered in this study.

As mentioned above, the basic objective of WFLO is energy output maximization, but when wind turbines are arranged to achieve this goal in a limited space, some wind turbines can experience greater wake effects than other turbines. Consequently,

Table 1
Categorization of literature by methodology for WFLO.

Category	Algorithm	Authors. year [ref.]	Computational domain
Heuristic	Genetic algorithm (GA)	Mosetti et al., 1994 [3]	Discrete
		Grady et al., 2005 [5]	Discrete
		Huang. 2007 [8]	Discrete
		Mora et al., 2007 [9]	Discrete
		Elkinton et al., 2008 [10]	Discrete
		Emami et al., 2010 [11]	Discrete
		Gonzalez et al., 2010 [12], 2018 [13]	Discrete
		Chen et al., 2013 [14], 2015 [15]	Discrete
		Rahbari et al., 2014 [16]	Discrete
		Gao et al., 2015 [17], 2016 [18]	Discrete
		Mayo et al., 2016 [19]	Continuous
		Sorkhabi et al., 2016 [20]	Continuous
		Wang et al., 2017 [21]	Continuous
		Pillai et al., 2017 [22]	Discrete, Continuous
		Song et al., 2017 [23]	Discrete
		Yin et al., 2017 [24]	Discrete
		Parada et al., 2017 [25]	Discrete
	Evolutionary strategy (ES)	Kusiak et al., 2010 [26], 2010 [27]	Continuous
		Song et al., 2016 [28]	Continuous
	Particle swarm optimization (PSO)	Wan et al., 2010 [29]	
		Chowdhury et al., 2012 [30], 2013 [31]	Continuous
		Pookpunt et al., 2013 [32]	Discrete
		Hou et al., 2016 [33], 2017 [34]	Continuous
		Pillai et al., 2017 [22]	Discrete, Continuous
	Ant colony optimization (ACO)	Eroğlu et al., 2012 [35]	Continuous
	Monte Carlo simulation (MCS)	Marmidis et al., 2008 [6]	Discrete
	Simulated annealing algorithm (SAA)	Rivas et al., 2009 [7]	Continuous
	Harmony search (HS)	Kallioras et al., 2015 [36]	Discrete
	Pattern search (PS)	Dupont et al., 2016 [37]	Continuous
	Random search (RS)	Wagner et al., 2013 [38]	Continuous
		Feng et al., 2015 [39], 2017 [40]	Continuous
	Greedy heuristic algorithm (GHA)	Ozturk et al., 2004 [4]	Continuous
		Elkinton et al., 2008 [10]	Discrete
		Chen et al., 2016 [41]	Discrete
Mathematical programming	Mixed integer programming (MIP)	Archer et al., 2011 [42]	Discrete
		Turner et al., 2014 [43]	Discrete
		Kuo et al., 2015 [44], 2016 [45]	Discrete
		MirHassani et al., 2017 [46]	Discrete
	Gradient-based optimization (GBO)	Park et al., 2015 [47]	Continuous
		Guirguis et al., 2016 [48], 2017 [49]	Continuous
		Tingey et al., 2017 [50]	Continuous
		King et al., 2017 [51]	Continuous

wind turbines exposed to high wake effects have decreased energy outputs due to their wind velocity deficits and increased fatigue loads due to increased turbulence of the flow into them, which can cause mechanical failure and shorten their life expectancies [45,55]. Therefore, the objective of this study was to maximize energy output while preventing specific wind turbines from being exposed to excessive wakes in the wind farm layout process. To that end, a new objective function for the WFLO problem was developed that can increase energy output while making the wake losses of the turbines on a wind farm uniform. This objective function adjusts the wake effects of all of the wind turbines on the wind farm to similar levels, thus promoting the stabilization of all of them. An SAA, which is a heuristic method, is used for the WFLO algorithm, and a discrete model is applied for the computational domain. Furthermore, a grid processing method for handling the irregular outer boundaries of actual wind farms in a discrete model was developed.

The rest of this paper is organized as follows. In Section 2, the wake model and equations for calculating the energy output are presented. Section 3 describes the layout optimization algorithm and the newly proposed objective function for making the wake losses uniform. Section 4 discusses the results obtained by implementing the proposed algorithm. Finally, Section 5 summarizes the conclusions.

2. Formulation

2.1. Estimation of annual energy production

The annual energy production (AEP) of a wind farm is defined as the sum of the hourly outputs from all of the wind turbines on the wind farm. To calculate this quantity, the speed probability distribution of the wind that blows to the wind farm and the wind turbine power corresponding to the wind speed are required. If the wind is divided into a number of intervals for all directions using the bin method and then into a number of wind speed intervals for each direction interval, the AEP can be expressed as follows [2]:

$$AEP = 8760 \sum_{i=1}^{N_t} \sum_{j=1}^{N_d} \sum_{k=1}^{N_s} F\left(u_{ijk}\right) P(u_{ik}) \tag{1}$$

where $F(u_{ijk})$ is the probability that wind in speed bin k will blow from turbine i to direction sector j, and $P(u_{ik})$ is the power of wind turbine i at wind speed bin k. The number 8760 is the annual number of hours based on 365 days per year. N_s is a number determined by dividing the operating wind speed range (typically 3–25 m/s) of a wind turbine by the wind speed interval. For the wind speed interval, 0.5 m/s is generally used. N_d is the total bearing divided by the direction interval. N_t is the total number of wind turbines to be installed.

2.2. Wake model

2.2.1. Single wake model

To analyze the wake effect, a mathematical model for calculating the wake of a single rotor is required first. In this study, the wind velocity deficit due to the wake effect in the downstream wind turbines was calculated using the Jensen wake model (originally proposed in Ref. [56], further developed by Katic et al. [57]), which is an analytical wake model. The Jensen wake model is known to be less accurate than the numerical wake model. However, it yields valid results for offshore wind farms and in the far wake areas of flat terrains. Therefore, and owing to its simple equations and fast calculations, it is widely used in WFLO research and many commercial software [52].

As shown in Fig. 1, the Jensen wake model assumes that the diameter of the wake extended to the back of the rotor increases linearly in proportion to the downstream distance x, and the wind speed inside the wake in the radial direction of the wake is identical. By the law of conservation of momentum inside the wake area, the Jensen wake model can be derived as follows:

$$D_r^2 u + \left(D_w^2 - D_r^2\right) u_0 = D_w^2 u_1 \tag{2}$$

where D_r is the turbine rotor diameter, u is the velocity behind the turbine, D_w is the diameter of the downstream wake, u_0 is free stream wind speed (undisturbed incoming wind velocity), and u_1 is the wake velocity at a downstream distance x. Using the relationship between axial induction factor and the thrust factor C_t, the wake velocity as a function of x can be defined as follows [57]:

$$u_1 = u_0\left[1 - \left(1 - \sqrt{1 - C_t}\right)\left(\frac{D_r}{D_r + 2k_w x}\right)^2\right] \tag{3}$$

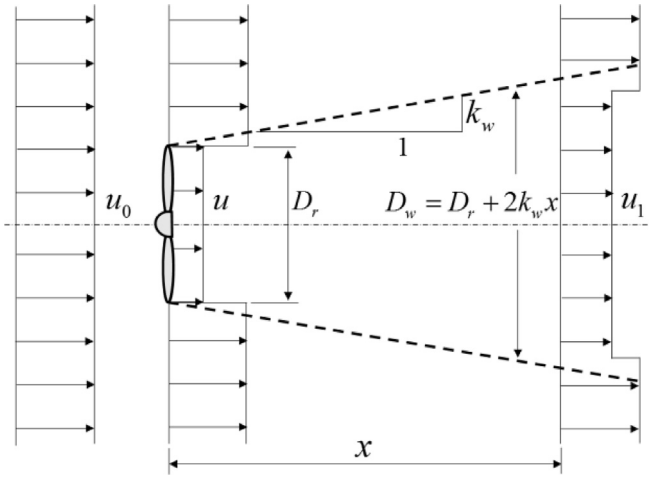

Fig. 1. Schematic representation of Jensen single wake model [57].

where k_w is the wake decay constant, which determines the size of the expanded wake behind the wind turbine. This wake decay constant can be calculated as a function of the surface roughness of the calculated area by using the following formula [52]:

$$k_w = \frac{0.5}{\ln(h_{hub}/z_0)} \tag{4}$$

where *hhub* is the hub height of the wind turbine and *z0* is the surface roughness height of the wind farm area. Because *z0* is difficult to calculate accurately, it generally depends on the judgment of the designer, but the empirical value recommended by the European Wind Atlas can also be used [58].

2.2.2. Multiple wake model

There are multiple turbines on wind farms, and they interact with one another in various ways depending on the wind direction and installed positions during operation or receive wake effects from one or more turbines, as shown in Fig. 2. Therefore, to consider the wake losses throughout a wind farm, the ranges of these multiple and superimposed wake effects and the resulting wind speed reduction due to the wake effects must be calculated.

Fig. 2 illustrates the wake effect according to wind direction on a wind farm. Depending on the wind direction, which is affected by the wake, the entire rotor area (Fig. 2(a)) or only part of the rotor area (Fig. 2(b)) may be affected by the wake. Therefore, according to the Jensen single wake model Eq. (3), the wind velocity deficit in a wind turbine subjected to the wake effect can be expressed using the ratio of the area swept by the rotor under the wake effect as follows [55]:

$$u_{def} = u_0\left(1 - \sqrt{1 - C_t}\right)\left(\frac{D_r}{D_r + 2k_w x}\right)^2 \frac{A_{overlap}}{A_r} \tag{5}$$

where $A_{overlap}$ is the overlap area between the expanded wake area A_w of the upstream wind turbine and the rotor swept area of the downstream wind turbine A_r, as shown in Fig. 3.

Fig. 3 illustrates the overlap area, which can be determined as follows. (1) Calculate the center (C_w) of the expanded wake at the downstream wind turbine and the wake diameter D_w based on x, as shown in Fig. 2(b). (2) Determine whether the rotor area overlaps with the expanded wake area or is fully included in the wake area. (3) Calculate the intersection area depending on whether overlapping or full inclusion occurs, as follows:

$$A_{overlap} = \begin{cases} 0, & \text{if } R_w + R_r \le d \\ A_r, & \text{if } R_w - R_r \ge d \\ A_{partial}, & \text{otherwise} \end{cases} \tag{6}$$

where R_w is the radius of the wake of the upstream wind turbine, R_r is the radius of the rotor of the downstream wind turbine, and d is the distance between the centers of the wake and rotor. $A_{partial}$ is the overlap area created by partial wake and can be calculated as follows from the area of the fan shape created by connection of the centers of the wake and rotor with the intersection points (p_1, p_2) of the two circles and the triangle that connects the intersection points, as shown in Fig. 3 [21]:

$$A_{partial} = \frac{1}{2}\left[R_w^2(\theta_w - \sin\theta_w) + R_r^2(\theta_r - \sin\theta_r)\right] \tag{7}$$

where θ_w and θ_r are the angles of the wake intersection arc and rotor intersection arc, respectively, and can be respectively expressed as follows:

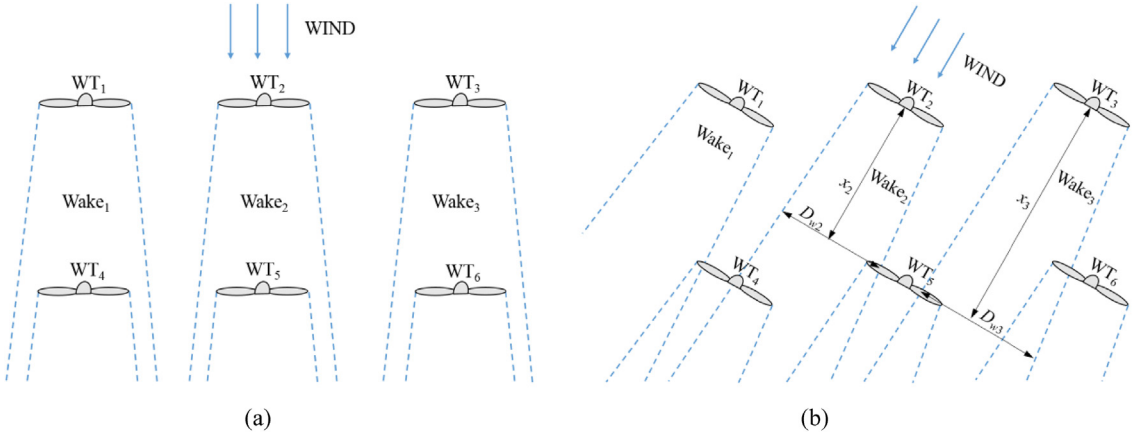

Fig. 2. Illustration of wake effect according to wind direction on a wind farm. (a) The entire wind turbine rotor area experiences the wake effect. (b) Only part of the wind turbine rotor area experiences the wake effect.

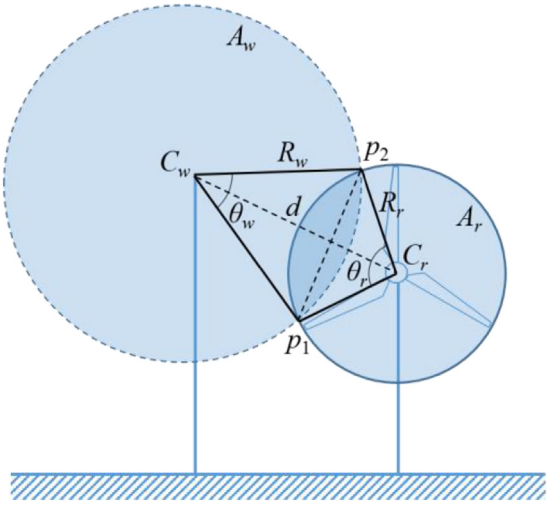

Fig. 3. Overlap between the wake area and wind turbine rotor swept area.

$$\theta_w = 2\cos^{-1}\left(\frac{d^2 + \left(R_w^2 - R_r^2\right)}{2dR_w}\right) \tag{8}$$

$$\theta_r = 2\cos^{-1}\left(\frac{d^2 - \left(R_w^2 - R_r^2\right)}{2dR_r}\right) \tag{9}$$

The wind velocity deficit resulting from multiple wakes, where one wind turbine i is subjected to wake effects from N wind turbines, can be calculated as follows [54]:

$$u_{mdef,i} = \sqrt{\sum_{i=1}^{N} u_{def,i}^2} \tag{10}$$

3. Methodology

3.1. Wind farm modeling

In this section, the optimization approach and objective function for WFLO are described. First, a discrete model was used for the computational domain to model the wind farm and handle the positional variables of the wind turbines, as shown in Fig. 4. This method is similar to the techniques used in previous studies, in which a wind farm area is divided into square cells and a wind turbine is placed at the center of each cell [3,5]. However, because the boundary of an actual wind farm is not rectangular, a method of modeling irregular wind farm boundaries is required in order to use a grid-based computational domain. In this study, the geometry of the outer boundary of the actual wind farm and that of an obstacle inside the wind farm were drawn on a grid, as shown in Fig. 4(a). Then, based on the results, the cells in which turbines could and could not be placed were specified using a flag variable, as shown in Fig. 4(b). This method is useful for cases with irregular boundaries, such as onshore wind farms, and helps avoid areas where no turbine can be placed, such as buildings or small reservoirs in wind farms, when performing layout optimization.

3.2. Optimization algorithm

The WFLO algorithm used in this study was an SAA, which is a representative stochastic optimization method. SAA is a method that is inspired by the annealing process in metallurgy in which a material is heated and then slowly cooled under controlled temperature conditions to change the position of the crystals inside the material so as to minimize internal energy. This has the effect of improving the strength and durability of the material [59]. The process of crystal relocation is the main reason SAA has been applied to the WFLO problem in this study. In the WFLO problem, wind turbines are compared to crystals and the wind farm is compared to the bulk material. Heat increases the energy of the crystals (wind turbines), allowing them to move freely; the slow cooling allows a new low-energy configuration (wake effect uniformity or energy maximization) to be discovered. The temperature is one of the computational parameters used for iterations and probability calculations during algorithm implementation to arrange wind turbines. The optimal solution is searched depending on the probability by varying this virtual temperature parameter [60].

Fig. 5 shows a flow chart of the SAA for the WFLO problem proposed in this report, and the main steps of the method and procedure for implementing this algorithm are as follows.

Step 1: Initialization of the wind turbine layout

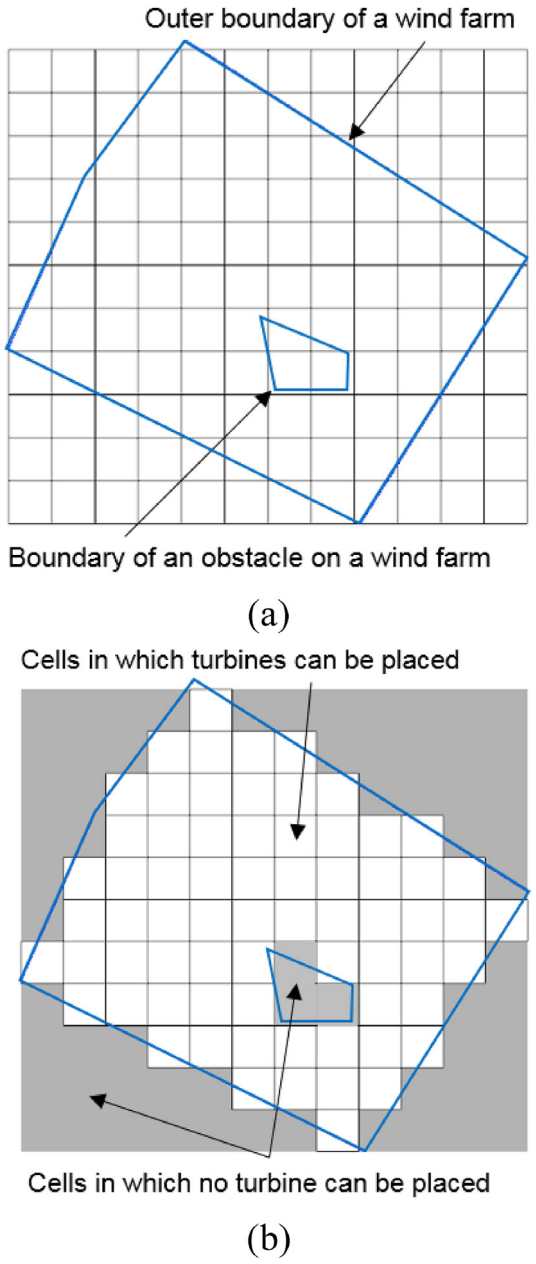

Fig. 4. Discrete method of modeling irregular wind farm boundaries. (a) Drawing of the outer boundary of an actual wind farm and the boundary of an obstacle on the wind farm on a grid. (b) Specification of cells in which turbines can and cannot be placed.

Theoretically, the initial solution does not have a significant effect on the SAA result. Therefore, the initial layout solution is generally determined randomly [59]. The initial temperature parameter may be set to 1.0 or lower depending on the characteristics of the problem.

Step 2: Perturbation of wind turbine position

Perturbation involves changing the positions of some turbines to find better positions and requires a perturbation strategy to improve the layout solution. As shown in Fig. 6, a two-step position change method was applied in this study. The first perturbation step is global positioning, in which the positions of the turbines for the entire wind farm are found, as shown in Fig. 6(a). The second is local positioning, in which the turbines are moved from their current positions to surrounding positions, as shown in Fig. 6(b). Global positioning was applied in 90% of the total algorithm performance, and local positioning was applied in the last 10% of the layout performance for fine tuning of the positions. Global positioning prevents dropping into local optima through broad space searching, and local positioning helps elucidate positions with higher energy efficiencies.

Step 3: Evaluation of the objective function

After perturbation, the value of the objective function of the obtained layout is calculated, and the candidate layout ($L_{candidate}$) is evaluated to determine whether this value is improved compared to that of the current layout ($L_{current}$). In this step, it is determined whether the candidate layout is accepted as the current layout using a cost function, in which the difference between the values of the objective function for the current and candidate layouts ($f_{current}$ and $f_{candidate}$, respectively) is calculated:

$$\Delta f = f_{current} - f_{candidate} \tag{11}$$

$$L_{current} = \begin{cases} L_{candidate}, & \Delta f < 0 \\ \text{go to step 4}, & \text{otherwise} \end{cases} \tag{12}$$

where Δf is the cost function. If its value is smaller than zero, that is, if the layout has improved, the candidate layout is accepted; otherwise, it is evaluated again using the Metropolis criterion in Step 4.

Step 4: Metropolis criterion

If the candidate layout is not accepted in Step 3, it is not discarded immediately, but rather is evaluated again using the Metropolis criterion to decide whether or not to accept it as the current layout. In this process, even if the value of the objective function of the candidate layout is lower than that of the current layout (i.e., the AEP of the candidate layout is lower than that of the current layout in terms of energy maximization), it is determined whether the candidate layout can be accepted as the current layout probabilistically. This characteristic of the SAA prevents convergence to local optima that may occur by following only improved solutions. The Metropolis criterion based on the Metropolis–Hastings algorithm is as follows [59]:

$$P_{metro} = \exp\left(-\frac{\Delta f}{T_c}\right) \tag{13}$$

$$L_{current} = \begin{cases} L_{candidate}, & \text{if } P_{metro} > P_{rand} \\ L_{current}, & \text{otherwise} \end{cases} \tag{14}$$

where P_{metro} is a metropolis probability, P_{rand} is a probability obtained using the random number generator function, and T_c is the current temperature parameter.

Step 5: Temperature control

This step involves gradually lowering the temperature parameter via a “cooling schedule.” This cooling schedule is an important factor affecting the efficiency of the SAA. A linearly fast temperature decrease increases the possibility of convergence to local optima, and a logarithmically slow decrease increases the performance

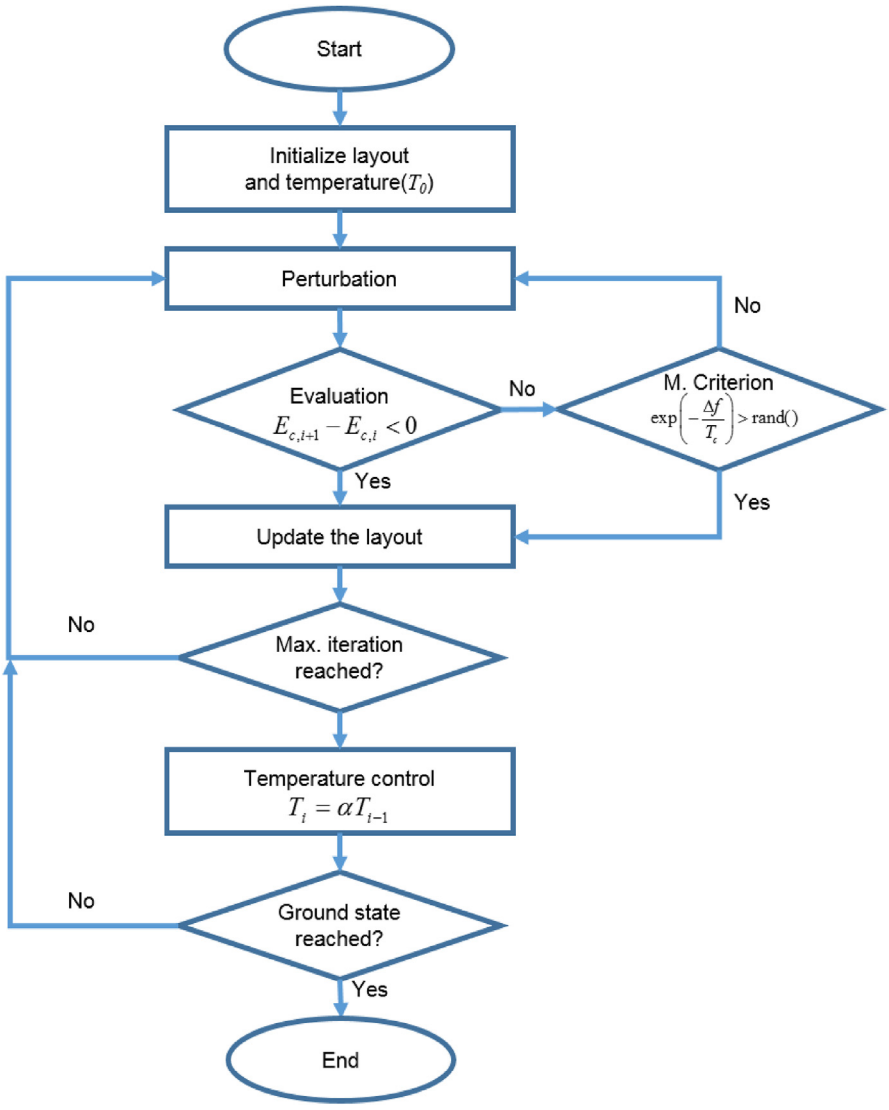

Fig. 5. Flow chart of the optimization algorithm process.

time. Therefore, the following practical method is often used [59]:

$$T_i = \alpha T_{i-1}\ (0.85 < \alpha < 0.96) \tag{15}$$

3.3. Objective function

In this study, objective functions for (1) energy maximization, which is the basic objective function for WFLO, and (2) making the wake losses uniform were developed and applied to layout optimization. The first objective function is for wind farm energy maximization and is defined by the ratio of net AEP (E_{net}), which considers the energy loss resulting from the wake effect, to the gross AEP (E_{gross}), which assumes no energy loss due to wake effect on the wind farm, as follows:

$$f_{energy,\max} = \frac{E_{net}}{E_{gross}} \tag{16}$$

Secondly, the new objective function proposed in this study aims to adjust the wake loss ratios of the individual turbines on the wind farm to similar levels. As mentioned in Section 1, if specific turbines on a wind farm are subjected to greater wake effects than other turbines, they are likely to cause more problems during operation and their design lives cannot be guaranteed. The proposed objective function that minimizes the standard deviation of the wake losses to which the turbines are subjected is as follows:

$$f_{wake,uniform} = 1 - \sqrt{\frac{1}{N_t}\sum_{i=1}^{N_t}(w_a - w_i)^2} \tag{17}$$

where w_a is the average wake loss, w_i is the wake loss of each wind turbine, and N_t is the number of wind turbines on the wind farm.

The purpose of minimizing the standard deviation of the wake losses is to reduce the wake loss differences between turbines to prevent the concentration of wake effects on specific turbines.

4. Case study: Gasiri wind farm

This section describes the implementation of WFLO for Gasiri wind farm using the two types of objective functions mentioned above and presents a comparison of the results.

Gasiri wind farm is in operation on Jeju Island in the south of

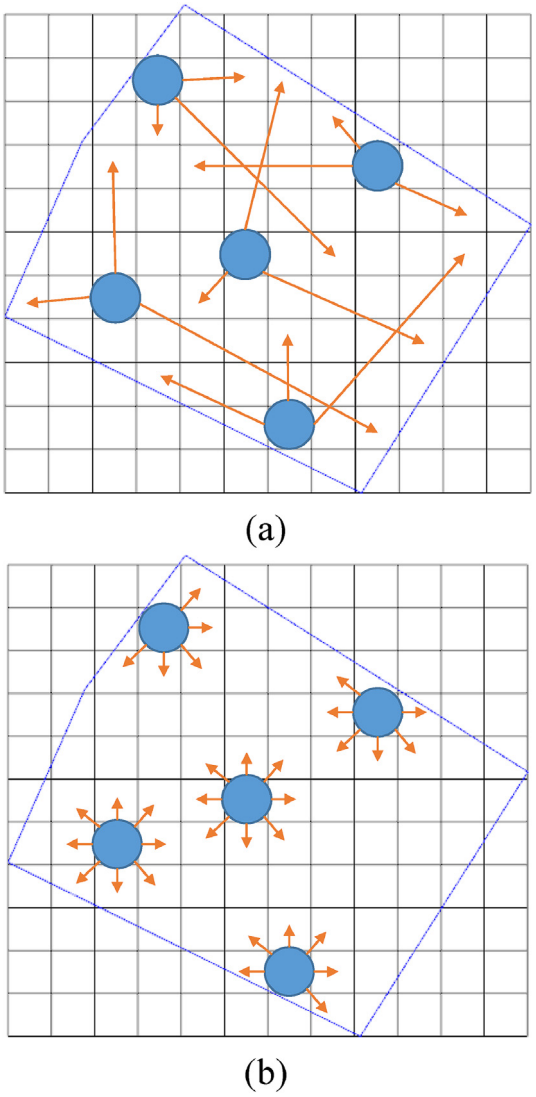

Fig. 6. Perturbation steps to search promising location of wind turbines. (a) Global positioning method. (b) Local positioning method.

Korea. Fig. 7 shows the configuration of the wind turbines on Gasiri wind farm and the wind rose at a height of 70 m measured in the meteorological mast near Gasiri wind farm. On Gasiri wind farm, there are six 750 kW (HS50, U50) wind turbines and seven 1500 kW wind turbines (HJWT77), and the total capacity of the farm is 15,000 kW. As shown in Fig. 7, the prevailing wind direction on the wind farm is NNW, and all 13 wind turbines are placed in a grid pattern based on this direction. Table 2 summarizes the specifications of the three types of wind turbines on Gasiri wind farm.

4.1. AEP validation

To verify the reliability of the WFLO results, accurate calculation of the wind farm AEP is required. To that end, computer code was developed to calculate the actual AEP of the farm using measured wind data, as shown in Fig. 8. And the AEP calculation results for Gasiri wind farm were compared with the power production data collected from the Gasiri wind farm wind turbines.

Fig. 9 compares the computed and actual AEPs for each wind turbine. The 750 kW wind turbines are excluded because the data

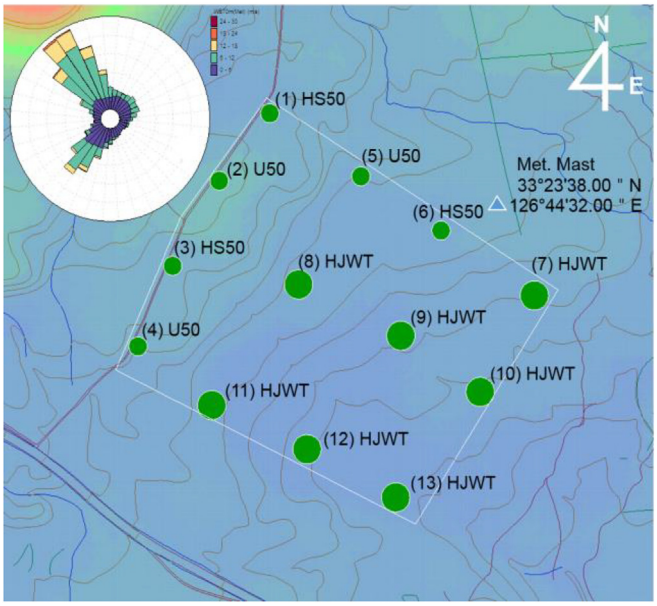

Fig. 7. Wind farm layout and wind rose of Gasiri wind farm.

Table 2
Specifications of the three types of wind turbines on Gasiri wind farm.

Wind turbines	HS50	U50	HJWT77
Rated power (kW)	750	750	1500
Hub height (m)	50	50	70
Rotor diameter (m)	50	50	77
Cut-in wind speed (m/s)	3.5	3	3.5
Rated wind speed (m/s)	12	12.5	13
Cut-out wind speed (m/s)	25	25	25

collected from some of them showed a low recovery rate. In the actual AEP results in Fig. 9, wind turbines with the same capacity show different power outputs. There may be various reasons for these differences in power production, but the variation in wake loss with on the turbine position can be seen as a factor that has a substantial effect on these power production differences. The computed AEPs show a trend similar to that of the AEPs for the actual wind turbines; thus, the computed AEPs reflect the wake losses of each wind turbine well. Table 3 summarizes the data collected from the wind turbines and the AEP calculation results. The total AEP calculated for seven wind turbines is 24.06 GWh, which is 0.86 GWh greater than the actual AEP of 23.2 GWh. The cause of this difference could be related to the actual operation of the wind turbine, but the main cause seems to be the error in the calculations with the wake model.

4.2. Layout optimization

Gasiri wind farm was rearranged to verify the performance of the proposed layout optimization algorithm. Since the purpose of this study was to optimize the process of deciding the specific positions of wind turbines after the types and numbers of wind turbines to be installed on the farm are selected, layout optimization for energy maximization (LOEM) and layout optimization for wake effect uniformity (LOWU) were performed under the same conditions without changing the types and numbers of wind turbines in the Gasiri wind farm using the two types of objective functions mentioned above, and the results were compared.

Fig. 10 shows the wind farm computational domain for layout

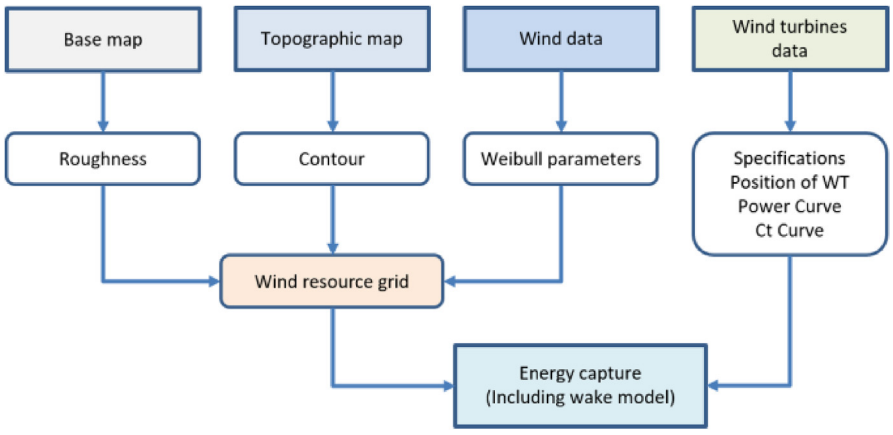

Fig. 8. Flowchart of the developed code for calculating the AEP of the wind farm.

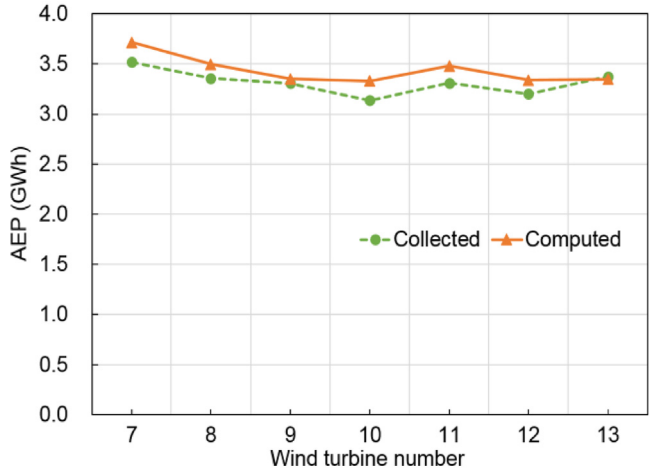

Fig. 9. Comparison of the AEPs collected from Gasiri wind farm with the computed AEPs. All of the compared wind turbines have capacities of 1500 kW.

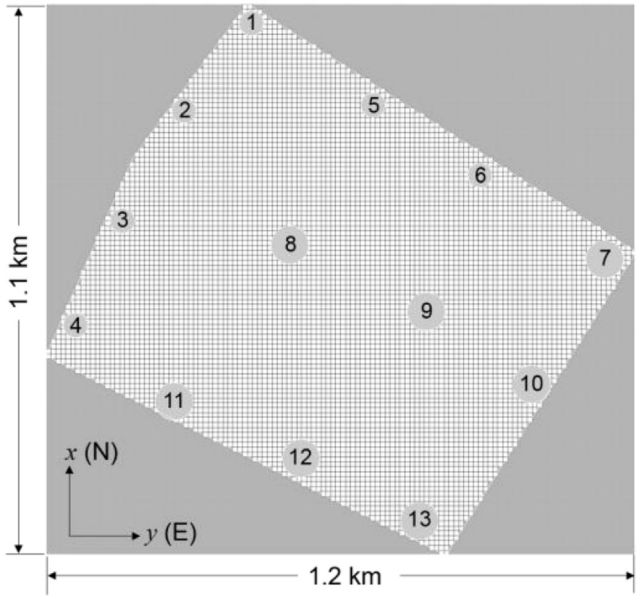

Fig. 10. Wind farm domain and coordinates for layout optimization. Circles and numbers indicate the positions and numbers of the existing wind turbines in the Gasiri wind farm.

optimization and the existing wind turbine positions. The total domain area is 1.2 × 1.1 km based on the boundaries of Gasiri wind farm. The area for locating the wind turbines was divided into 120 × 110 cells with dimensions of 10 × 10 m to improve the degree of freedom of placement, and the cells were divided into placement-allowed cells and placement-prohibited cells. The *x* and *y* axes of the coordinate system were north and east, respectively, based on the azimuth rotation direction. The minimum spacing between wind turbines was set to 230 m to maintain the minimum of 3D (rotor diameter) considering the largest wind turbine rotor size (HJWT77) on Gasiri wind farm.

The temperature parameter was determined based on the preliminary performance. For the initial temperature, 0.05 was applied because the solutions only fluctuated without improvement until approximately 0.05, because a high-temperature parameter increased the probability of selecting a worse solution. For the stopping temperature, a sufficiently low value is required, and a marginal area in which there is no improvement in the final solution even after long-time performance was found based on the preliminary performance and applied. The related parameters are listed in Table 4.

Fig. 11 shows the variations of the values of the two objective functions in the total performance process of the algorithm. These values improve and converge to certain value, although they fluctuate frequently in the early stage. In the early stage of the algorithm, various layouts are tested for the entire farm area with a high probability of movement when the temperature parameter is high, and the layout is stabilized as the temperature decreases. This behavior clearly shows the characteristics of the SAA. The LOEM has

Table 3
Comparison of the AEPs collected from Gasiri wind farm with the computed AEPs.

Wind turbine number		7	8	9	10	11	12	13	Total	Difference
AEP (GWh)	Collected	3.52	3.36	3.31	3.14	3.31	3.2	3.37	23.2	-
	Computed	3.72	3.5	3.35	3.33	3.48	3.34	3.35	24.06	0.86

Table 4
Parameters of the optimization algorithm for the WFLO problem.

Parameter	Value
Grid size (m)	1200 × 1100
Cell size (m)	10 × 10
Minimum spacing (m)	230
Initial temperature (−)	0.05
Stopping temperature (−)	0.0001
Temperature control (α)	0.95

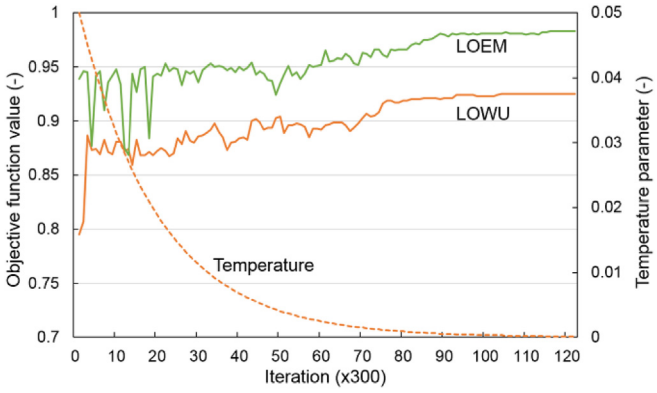

Fig. 11. Variation of the value of the objective function in WFLO.

a high applicability value, which is due to the relative size of the value of the objective function and is not related to the efficiency of the optimal layout.

The layout optimization results obtained using the proposed algorithm are shown in Fig. 12 and summarized in Table 5. Fig. 12(a) compares the wind turbine positions in the LOEM results with the existing layout. In the LOEM layout, the high-capacity wind turbines have moved to the front of the prevailing wind direction compared to their positions in the existing layout. Consequently, as shown in Fig. 12(b), the AEPs of the low-capacity wind turbines (nos. 1–6) decreased, whereas those of high-capacity wind turbines (nos. 7–13) increased. As can be seen in Table 5, as the total wake loss of the farm decreased by 4.72%, the net AEP increased by 2.42 GWh compared to that of the existing layout. This difference is due to the greater gain from reducing the wake loss of high-capacity wind turbines than low-capacity wind turbines because the former are placed in the front in the prevailing wind direction.

Fig. 12(c) shows the LOWU results, and the layout is slightly different from the LOEM layout. In the LOEM case, the low-capacity wind turbines are located at the back of the wind farm in relation to the prevailing wind direction, but in the LOWU results, some of them are located in front of the prevailing wind direction. Consequently, the AEPs of low-capacity wind turbines 5 and 6 increased, while those of high-capacity wind turbines 9 and 10 decreased compared to those in the LOEM results, as shown in Fig. 12(d). The net AEP of the total wind farm is 0.46 GWh lower than that in the LOEM case, but 1.96 GWh higher than that with the existing layout. However, the LOWU has additional advantages for the wake effects to which the individual wind turbines are subjected.

Fig. 13 compares the wake losses and standard deviations of the losses for each wind turbine among the existing layout and those obtained using the LOEM and LOWU. It can be seen that with the existing layout and that resulting from using the LOEM, there are turbines with 15% or higher wake losses (nos. 2, 6, 9, and 10), but the LOWU does not yield such turbines. Thus, although the LOEM produced the highest AEP, some wind turbines are exposed to high wake effects. In particular, these effects are concentrated on low-capacity wind turbines, because the LOEM performed layout optimization to increase the total energy while sacrificing some wind turbines that produced little energy. This choice is correct from the perspective of energy maximization but needs to be reviewed in terms of long-term wind farm operation. On the other hand, the

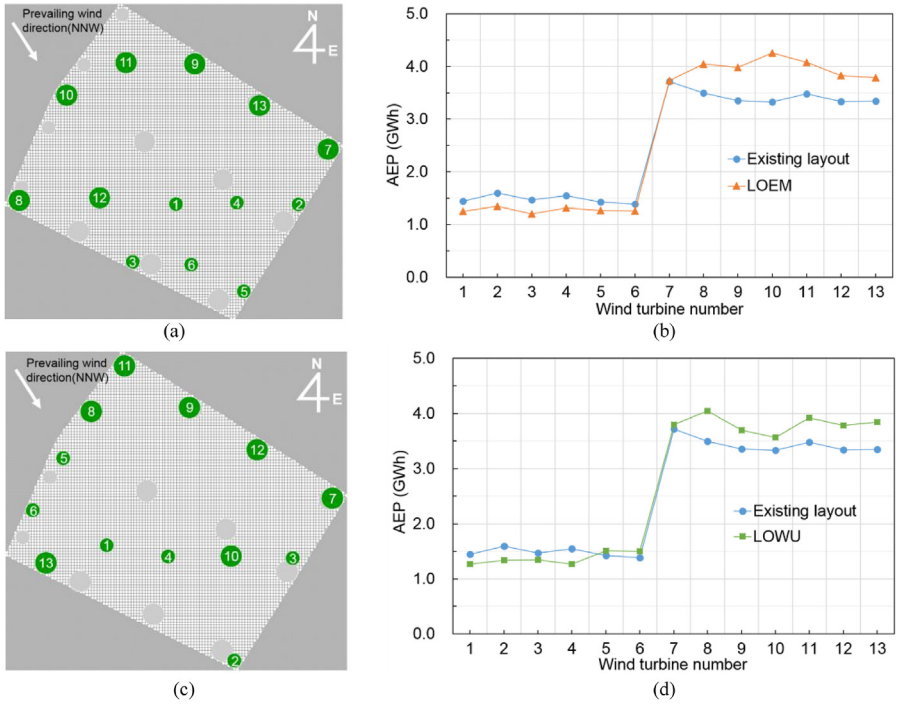

Fig. 12. Gasiri WFLO results obtained using two objective functions. (a) LOEM results. (b) Comparison of AEPs between LOEM and existing layout. (c) LOWU results. (d) Comparison of AEPs between LOWU and existing layout.

Table 5
Comparison of AEPs and wake losses among LOEM, LOWU, and existing layout.

Wind turbine number	net AEP/gross AEP (GWh)			Wake loss (%)		
	Existing layout	LOEM	LOWU	Existing layout	LOEM	LOWU
1	1.45/1.52	1.25/1.41	1.27/1.42	5.16	11.35	10.70
2	1.59/1.69	1.35/1.55	1.34/1.49	5.72	12.91	10.23
3	1.47/1.56	1.20/1.40	1.35/1.51	6.13	14.57	10.43
4	1.54/1.58	1.31/1.50	1.27/1.42	2.32	12.74	10.52
5	1.42/1.55	1.26/1.46	1.51/1.66	8.13	13.77	8.77
6	1.38/1.54	1.26/1.40	1.50/1.59	10.06	9.79	5.43
7	3.72/4.15	3.73/4.18	3.79/4.18	10.39	10.72	9.28
8	3.50/4.06	4.04/4.15	4.05/4.43	13.87	2.67	8.59
9	3.35/4.00	3.98/4.17	3.69/4.17	16.17	4.68	11.49
10	3.33/4.05	4.26/4.42	3.56/3.97	17.83	3.65	10.31
11	3.48/4.00	4.08/4.33	3.92/4.23	13.04	5.86	7.52
12	3.34/3.88	3.83/4.01	3.78/4.20	13.87	4.59	10.07
13	3.35/3.91	3.79/4.20	3.84/4.13	14.38	9.72	6.90
Total	32.92/37.50	35.34/38.20	34.88/38.41	12.21	7.49	9.19
Difference	-	+2.42	+1.96	-	−4.72	−3.02

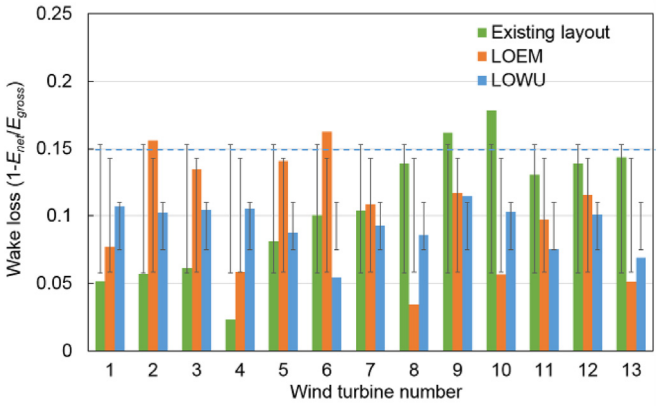

Fig. 13. Comparison of wake losses and standard deviations by wind turbine among the layouts obtained using the LOEM and LOWU and the existing layout.

LOWU yielded a slightly lower AEP than the LOEM, but the difference is only 0.46 GWh, and the LOWU shows generally uniform wake losses, as can be confirmed by the standard deviations of the wake losses. The standard deviations of the wake losses in the existing, LOEM, and LOWU cases are $STD_{Existing} = 4.58\%$, $STD_{LOEM} = 4.01\%$, and $STD_{LOWU} = 1.68\%$, respectively (Table 6). Thus, the standard deviation in the LOWU case is less than half of the other two values.

The wake effect in each direction on the wind farm was examined through the wake loss by bearing. Fig. 14 shows the wake losses by bearing in 36 directions on the wind farm. The existing layout generates 40% or higher wake losses at 120°, and the LOEM generates high wake losses at 90°. Thus, multiple wind turbines are subjected to wake effects when the wind blows from a specific direction and wake effect review for all bearings is necessary. On the other hand, the LOWU does not show marked peak points compared to the other layouts, suggesting that the LOWU distributes the wake effects to all bearings on the wind farm.

Table 6 compares the final results for the existing layout and the optimized layouts obtained using the two objective functions. Both layout optimization methods enabled the basic goal of WFLO to be achieved by improving the AEP while reducing the wake losses compared to those in the existing layout. In the LOWU case, the maximum wake loss is the lowest, at 11.49%, confirming that this method prevented the wake effects from being concentrated on specific turbine s. Moreover, the LOWU yielded wake losses with the smallest standard deviation, suggesting that the wake effects of the wind turbines throughout the entire wind farm were made uniform. However, the AEP produced by the LOWU was 0.46 GWh lower than that resulting from using the LOEM, indicating a somewhat lower efficiency in terms of energy maximization. Nonetheless, the LOWU contributed to stabilizing the overall wind turbine operation by making the wake losses of the individual wind turbines uniform.

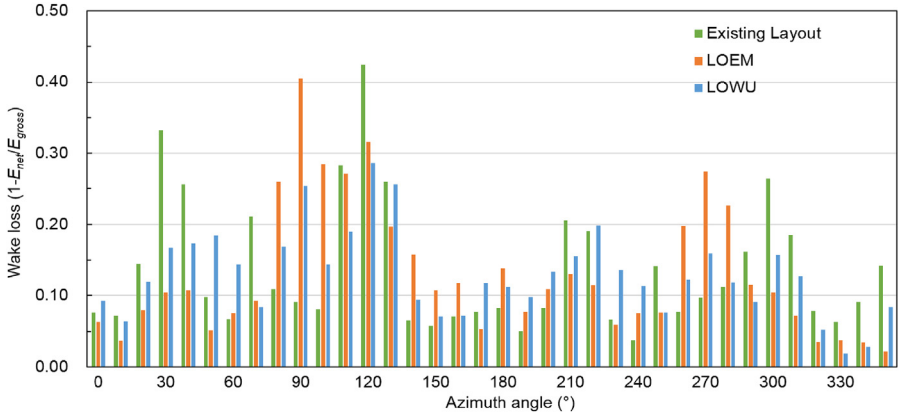

Fig. 14. Comparison of wake losses by direction among the LOEM, LOWU, and existing layout in the Gasiri wind farm.

Table 6
Comparison of final results of layout optimization among the existing layout and the optimized layouts obtained using the two objective functions.

Layout	AEP (GWh)	Wake loss (%)	Max. wake loss (%)	STD. wake loss (%)
Existing layout	32.92	12.21	17.83	4.58
LOEM	35.34	7.49	14.57	4.01
LOWU	34.88	9.19	11.49	1.68

5. Conclusions

In this study, a new objective function for making the wake effects of individual wind turbines uniform was developed and tested for WFLO. An SAA was used for layout optimization, and its performance was verified for an actual wind farm using an objective function for energy maximization, as well as the proposed objective function.

The AEP was calculated for optimization evaluation with no special assumptions about the wind using the wind data obtained from a meteorological mast on an actual wind farm. Furthermore, to verify the accuracy of the AEP before optimization, the calculated AEP was validated by comparing it with the annual power generated by an actual wind farm.

The LOEM produced the highest AEP, but the wake losses had a high standard deviation. On the other hand, the LOWU produced an AEP slightly lower than that of the LOEM but showed a higher energy output than the existing layout and wake losses with the lowest standard deviation. Furthermore, the AEP of the LOWU was not much different from that of the LOEM. In conclusion, although the LOWU yielded a lower energy output than the LOEM, the difference was small, and the LOWU prevented wake effect concentration on specific turbines by making these effects uniform.

The review of the wake losses by bearing confirmed that the wake effects primarily occurred in specific directions, which was due to the wind farm layout, and the LOWU approach proposed in this study made the wake effects uniform across bearings as well. Therefore, the objective function that made the wake losses uniform not only made the wake effects of the individual wind turbines uniform, but also made the wake effects uniform in all wind directions.

Because wind turbines are installed in limited spaces on most onshore wind farms, it is necessary to consider the wake effects in the layout, and the excessive wake effects of specific wind turbines must be examined. The wake effect differences increase when wind turbines of different hub heights and capacities are placed together. Since the proposed objective function does not simultaneously meet the two goals of maximizing energy and minimizing the wake loss standard deviation, techniques such as multi-objective optimization will need to be applied in future studies to achieve these conflicting objectives. However, the proposed algorithm is expected to provide a method of achieving long-term stable wind farm operation through effective design.

Acknowledgements

This work was supported by the Korea Institute of Energy Technology Evaluation and Planning (KETEP) grant funded by the Ministry of Trade, Industry and Energy (MOTIE) of the South Korean government (NO. 20164030201230 and NO. 20173010025010). The authors gratefully acknowledge the financial support provided by the KETEP and MOTIE.

References

[1] Hau E, von Renouard H. Wind turbines. second ed. Berlin: Springer; 2006. https://doi.org/10.1007/3-540-29284-5.
[2] Manwell JF, McGowan JG, Rogers AL. Wind energy explained. Wiley; 2009. https://doi.org/10.1002/9781119994367.
[3] Mosetti G, Poloni C, Diviacco B. Optimization of wind turbine positioning in large windfarms by means of a genetic algorithm. J Wind Eng Ind Aerodyn 1994;51:105–16. https://doi.org/10.1016/0167-6105(94)90080-9.
[4] Ozturk UA, Norman BA. Heuristic methods for wind energy conversion system positioning. Electr Power Syst Res 2004;70:179–85. https://doi.org/10.1016/j.epsr.2003.12.006.
[5] Grady SA, Hussaini MY, Abdullah MM. Placement of wind turbines using genetic algorithms. Renew Energy 2005;30:259–70. https://doi.org/10.1016/j.renene.2004.05.007.
[6] Marmidis G, Lazarou S, Pyrgioti E. Optimal placement of wind turbines in a wind park using Monte Carlo simulation. Renew Energy 2008;33:1455–60. https://doi.org/10.1016/j.renene.2007.09.004.
[7] Rivas RA, Clausen J, Hansen KS, Jensen LE. Solving the turbine positioning problem for large offshore wind farms by simulated annealing. Wind Eng 2009;33:287–97. https://doi.org/10.1260/0309-524X. 33.3.287.
[8] Huang H-S. Distributed genetic algorithm for optimization of wind farm annual profits. In: Intell syst appl to power syst 2007 ISAP 2007 int conf; 2007. p. 418–23. https://doi.org/10.1109/ISAP.2007.4441654.
[9] Castro Mora J, Calero Barón JM, Riquelme Santos JM, Burgos Payán M. An evolutive algorithm for wind farm optimal design. Neurocomputing 2007;70:2651–8. https://doi.org/10.1016/j.neucom.2006.05.017.
[10] Elkinton CN, Manwell JF, McGowan JG. Algorithms for offshore wind farm layout optimization. Wind Eng 2008;32:67–84. https://doi.org/10.1260/030952408784305877.
[11] Emami A, Noghreh P. New approach on optimization in placement of wind turbines within wind farm by genetic algorithms. Renew Energy 2010;35:1559–64. https://doi.org/10.1016/j.renene.2009.11.026.
[12] González JS, Gonzalez Rodriguez AG, Mora JC, Santos JR, Payan MB. Optimization of wind farm turbines layout using an evolutive algorithm. Renew Energy 2010;35:1671–81. https://doi.org/10.1016/j.renene.2010.01.010.
[13] Serrano González J, Burgos Payán M, Riquelme Santos JM. Optimal design of neighbouring offshore wind farms: a co-evolutionary approach. Appl Energy 2018;209:140–52. https://doi.org/10.1016/j.apenergy. 2017.10.120.
[14] Chen Y, Li H, Jin K, Song Q. Wind farm layout optimization using genetic algorithm with different hub height wind turbines. Energy Convers Manag 2013;70:56–65. https://doi.org/10.1016/j.enconman.2013.02.007.
[15] Chen Y, Li H, He B, Wang P, Jin K. Multi-objective genetic algorithm based innovative wind farm layout optimization method. Energy Convers Manag 2015;105:1318–27. https://doi.org/10.1016/j.enconman.20 15.09.011.
[16] Rahbari O, Vafaeipour M, Fazelpour F, Feidt M, Rosen MA. Towards realistic designs of wind farm layouts: application of a novel placement selector approach. Energy Convers Manag 2014;81:242–54. https://doi.org/10.1016/j.enconman.2014.02.010.
[17] Gao X, Yang H, Lin L, Koo P. Wind turbine layout optimization using multi-population genetic algorithm and a case study in Hong Kong offshore. J Wind Eng Ind Aerodyn 2015;139:89–99. https://doi.org/10.1016/j.jweia.2015.01.018.
[18] Gao X, Yang H, Lu L. Optimization of wind turbine layout position in a wind farm using a newly-developed two-dimensional wake model. Appl Energy 2016;174:192–200. https://doi.org/10.1016/j.apenergy.2016.04.098.
[19] Mayo M, Daoud M. Informed mutation of wind farm layouts to maximise energy harvest. Renew Energy 2016;89:437–48. https://doi.org/10.1016/j.renene.2015.12.006.
[20] Yamani Douzi Sorkhabi S, Romero DA, Yan GK, Gu MD, Moran J, Morgenroth M, et al. The impact of land use constraints in multi-objective energy-noise wind farm layout optimization. Renew Energy 2016;85:359–70. https://doi.org/10.1016/j.renene.2015.06.026.
[21] Wang L, Cholette ME, Tan ACC, Gu Y. A computationally-efficient layout optimization method for real wind farms considering altitude variations. Energy 2017;132:147–59. https://doi.org/10.1016/j.energy.2017. 05.076.
[22] Pillai AC, Chick J, Khorasanchi M, Barbouchi S, Johanning L. Application of an offshore wind farm layout optimization methodology at Middelgrunden wind farm. Ocean Eng 2017;139:287–97. https://doi.org/10.1016/j.oceaneng.2017.04.049.
[23] Song M, Wen Y, Duan B, Wang J, Gong Q. Micro-siting optimization of a wind farm built in multiple phases. Energy 2017;137:95–103. https://doi.org/10.1016/j.energy.2017.06.127.
[24] Yin PY, Wu TH, Hsu PY. Risk management of wind farm micro-siting using an enhanced genetic algorithm with simulation optimization. Renew Energy 2017;107:508–21. https://doi.org/10.1016/j.renene.2017.02.036.
[25] Parada L, Herrera C, Flores P, Parada V. Wind farm layout optimization using a Gaussian-based wake model. Renew Energy 2017;107:531–41. https://

doi.org/10.1016/j.renene.2017.02.017.
[26] Kusiak A, Song Z. Design of wind farm layout for maximum wind energy capture. Renew Energy 2010;35:685–94. https://doi.org/10.1016/j.renene.2009.08.019.
[27] Kusiak A, Zheng H. Optimization of wind turbine energy and power factor with an evolutionary computation algorithm. Energy 2010;35:1324–32. https://doi.org/10.1016/j.energy.2009.11.015.
[28] Song Z, Zhang Z, Chen X. The decision model of 3-dimensional wind farm layout design. Renew Energy 2016;85:248–58. https://doi.org/10.1016/j.renene.2015.06.036.
[29] Wan C, Wang J, Yang G, Zhang X. Particle swarm optimization based on Gaussian mutation and its application to wind farm micro-siting. In: 49th IEEE conf decis control; 2010. p. 2227–32. https://doi.org/10.1109/CDC.2010.5716941.
[30] Chowdhury S, Zhang J, Messac A, Castillo L. Unrestricted wind farm layout optimization (UWFLO): investigating key factors influencing the maximum power generation. Renew Energy 2012;38:16–30. https://doi.org/10.1016/j.renene.2011.06.033.
[31] Chowdhury S, Zhang J, Messac A, Castillo L. Optimizing the arrangement and the selection of turbines for wind farms subject to varying wind conditions. Renew Energy 2013;52:273–82. https://doi.org/10.1016/j.renene.2012.10.017.
[32] Pookpunt S, Ongsakul W. Optimal placement of wind turbines within wind farm using binary particle swarm optimization with time-varying acceleration coefficients. Renew Energy 2013;55:266–76. https://doi.org/10.1016/j.renene.2012.12.005.
[33] Hou P, Hu W, Chen C, Soltani M, Chen Z. Optimization of offshore wind farm layout in restricted zones. Energy 2016;113:487–96. https://doi.org/10.1016/j.energy.2016.07.062.
[34] Hou P, Hu W, Soltani M, Chen C, Chen Z. Combined optimization for offshore wind turbine micro siting. Appl Energy 2017;189:271–82. https://doi.org/10.1016/j.apenergy.2016.11.083.
[35] Eroğlu Y, Seçkiner SU. Design of wind farm layout using ant colony algorithm. Renew Energy 2012;44:53–62. https://doi.org/10.1016/j.renene. 2011.12.013.
[36] Kallioras NA, Lagaros ND, Karlaftis MG, Pachy P. Optimum layout design of onshore wind farms considering stochastic loading. Adv Eng Software 2015;88:8–20. https://doi.org/10.1016/j.advengsoft.2015.05.002.
[37] DuPont B, Cagan J, Moriarty P. An advanced modeling system for optimization of wind farm layout and wind turbine sizing using a multi-level extended pattern search algorithm. Energy 2016;106:802–14. https://doi.org/10.1016/j.energy.2015.12.033.
[38] Wagner M, Day J, Neumann F. A fast and effective local search algorithm for optimizing the placement of wind turbines. Renew Energy 2013;51:64–70. https://doi.org/10.1016/j.renene.2012.09.008.
[39] Feng J, Shen WZ. Solving the wind farm layout optimization problem using random search algorithm. Renew Energy 2015;78:182–92. https://doi.org/10.1016/j.renene.2015.01.005.
[40] Feng J, Shen WZ. Design optimization of offshore wind farms with multiple types of wind turbines. Appl Energy 2017;205:1283–97. https://doi.org/10.1016/j.apenergy.2017.08.107.
[41] Chen K, Song MX, Zhang X, Wang SF. Wind turbine layout optimization with multiple hub height wind turbines using greedy algorithm. Renew Energy 2016;96:676–86. https://doi.org/10.1016/j.renene. 2016.05.018.
[42] Archer R, Nates G, Donovan S, Waterer H. Wind turbine interference in a wind farm layout optimization mixed integer linear programming model. Wind Eng 2011;35:165–75. https://doi.org/10.1260/0309-524X.35.2.165.
[43] Turner SDO, Romero DA, Zhang PY, Amon CH, Chan TCY. A new mathematical programming approach to optimize wind farm layouts. Renew Energy 2014;63:674–80. https://doi.org/10.1016/j.renene.2013.10.023.
[44] Kuo JYJ, Romero DA, Amon CH. A mechanistic semi-empirical wake interaction model for wind farm layout optimization. Energy 2015;93:2157–65. https://doi.org/10.1016/j.energy.2015.10.009.
[45] Kuo JYJ, Romero DA, Beck JC, Amon CH. Wind farm layout optimization on complex terrains – integrating a CFD wake model with mixed-integer programming. Appl Energy 2016;178:404–14. https://doi.org/10.1016/j.apenergy.2016.06.085.
[46] MirHassani SA, Yarahmadi A. Wind farm layout optimization under uncertainty. Renew Energy 2017;107:288–97. https://doi.org/10.1016/j.renene.2017.01.063.
[47] Park J, Law KH. Layout optimization for maximizing wind farm power production using sequential convex programming. Appl Energy 2015;151:320–34. https://doi.org/10.1016/j.apenergy.2015.03.139.
[48] Guirguis D, Romero DA, Amon CH. Toward efficient optimization of wind farm layouts: utilizing exact gradient information. Appl Energy 2016;179:110–23. https://doi.org/10.1016/j.apenergy.2016.06.101.
[49] Guirguis D, Romero DA, Amon CH. Gradient-based multidisciplinary design of wind farms with continuous-variable formulations. Appl Energy 2017;197:279–91. https://doi.org/10.1016/j.apenergy.2017.04.030.
[50] Tingey EB, Ning A. Trading off sound pressure level and average power production for wind farm layout optimization. Renew Energy 2017;114:547–55. https://doi.org/10.1016/j.renene.2017.07.057.
[51] King RN, Dykes K, Graf P, Hamlington PE. Optimization of wind plant layouts using an adjoint approach. Wind Energy Sci. 2017;2:115–31. https://doi.org/10.5194/wes-2-115-2017.
[52] Serrano González J, Burgos Payán M, Santos JMR, González-Longatt F. A review and recent developments in the optimal wind-turbine micro-siting problem. Renew Sustain Energy Rev 2014;30:133–44. https://doi.org/10.1016/j.rser.2013.09.027.
[53] Rodrigues S, Bauer P, PAN Bosman. Multi-objective optimization of wind farm layouts – complexity, constraint handling and scalability. Renew Sustain Energy Rev 2016;65:587–609. https://doi.org/10.1016/j.rser. 2016.07.021.
[54] Pérez B, Mínguez R, Guanche R. Offshore wind farm layout optimization using mathematical programming techniques. Renew Energy 2013;53:389–99. https://doi.org/10.1016/j.renene.2012.12.007.
[55] Mittal P, Kulkarni K, Mitra K. A novel hybrid optimization methodology to optimize the total number and placement of wind turbines. Renew Energy 2016;86:133–47. https://doi.org/10.1016/j.renene. 2015.07.100.
[56] Jensen NO. A note on wind generator interaction. Technical. Roskilde, Denmark: Risø National Laboratory; 1983.
[57] Katic I, Højstrup J, Jensen NO. A simple model for cluster efficiency. Eur Wind Energy Assoc Conf Exhib; 1986. p. 407–10.
[58] Troen I, Lundtang Petersen E. European wind atlas. Risø National Laboratory; 1989. https://doi.org/10.1016/0014-2999(86)90768-5.
[59] Du KL, Swamy MNS. Search and optimization by metaheuristics: techniques and algorithms inspired by nature. Search Optim by Metaheuristics Tech Algorithms Inspired by Nat 2016:1–434. https://doi.org/10.10.07/978-3-319-41192-7.
[60] Brownlee J. Clever algorithms. 2011. https://doi.org/10.10.17/CBO9781107415324.004.